Journal of Materials Chemistry C

Accepted Manuscript

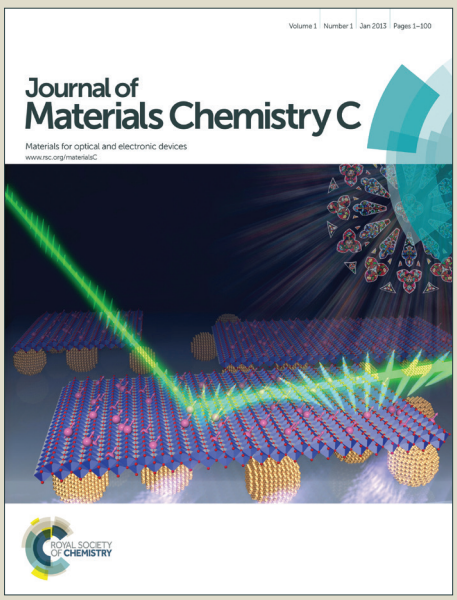

ROYAL SOCIETY OF CHEMISTRY

www.rsc.org/materialsC

Cite this: DOI: 10.1039/c0xx00000x

www.rsc.org/xxxxxx

ARTICLE TYPE

Formation of Persistent Ordered Lamellar Mesophases in Azobenzene-Containing Silver Thiolates and Their Implications for Controlled Synthesis of Silver Nanomaterials

Junfei Duan,[a,c] Jie Ma,[a] Bin Wu,[a] Qian Li,[a] Jianglin Fang[b] and Dongzhong Chen*[a]

Received (in XXX, XXX) Xth XXXXXXXXX 20XX, Accepted Xth XXXXXXXXX 20XX
DOI: 10.1039/b000000x

Metal thiolates have aroused intensive interests mainly due to their precursor-based preparation of nanostructured metal or metal chalcogenides. In this paper, a series of azobenzene-containing thiol ligands with different length alkoxy tails and their corresponding silver thiolates AgS-$C_{10}H_{21}$-Ph-N=N-Ph-OC_nH_{2n+1} with n = 1, 6, 8, 12, have been successfully synthesized, then their thermal properties and phase behavior have been systematically investigated by differential scanning calorimetry (DSC), variable-temperature SAXS/WAXS and temperature dependent FTIR. By introducing azobenzene mesogen for the first time into the silver thiolates, ordered lamellar liquid crystalline mesophases persisting throughout higher temperature have been achieved derived from their specific orthorhombic crystalline structures, which are in sharp contrast to the micellar or hexagonal columnar mesophases reported for silver alkane thiolates with longer aliphatic alkyl chain $AgSC_mH_{2m+1}$ ($m \geq 12$) owing to the interplay of azobenzene mesogen π-π stacking and the inorganic skeleton binding of Ag-S slab. Furthermore, the intermediate nanoparticles formation and silver nanodisks preparation through *in situ* thermolytic reaction based on such mesogenic precursors have been demonstrated in principle. As a kind of functional metallomesogen precursors the silver mesogenic thiolates with persistent ordered lamellar mesophases provide an ideal two-dimensional (2D) confined environment for the investigation of layered-precursor-to-lamellar-nanomaterial (LPLM) mechanism of solventless thermolysis and the fascinating controlled preparation of variant 2D shaped metal or metal sulfide nanomaterials.

1. Introduction

Metal thiolates combining the characteristic properties of metal atoms with design flexibility and fluidity of organic molecules have attracted considerable experimental and theoretical studies during the past decades.[1] Such as copper thiolates[2,3] and gold(I) thiolates[4-6] with highly ordered assembled structures facilitated the precursor based preparation of nanostructured metal or metal chalcogenides. Especially silver alkane thiolates with highly ordered layered quasihexagonal crystalline structure[7] exhibited rich thermotropic phase behavior.[8] Their thermotropic mesophases varied with the length of alkyl chain, but the melting points kept almost constant independent of the chain length.[9] More important, various metal or metal sulfide nanomaterials with controllable size and morphology have been prepared from the corresponding metal thiolate precursors through solvothermal[10] or solventless thermolysis.[11-18] Solventless thermolysis can be regarded as a quasi-solid-state process with the nucleation and subsequent growth relatively controllable and adjustable[18] and serve as an intriguing method for nanostructured materials preparation. Korgel and co-workers have reported the synthesis of Cu_2S,[11,12] NiS[13] and Bi_2S_3[14] by using corresponding thiolate precusors through solventless thermolysis approach. Wu and co-workers have prepared Cu_2S,[15] Bi,[16] PbS[17] and Ag[18] nanoproducts by this same method based on alkane thiolate precursors and, consequently, they proposed a possible mechanism of the metal thiolates based layered-precusor-to-lamellar-nanoproduct.[15-18] Some intermediates such as small nanoparticle aggregation for Cu_2S nanodisks[15b] or bismuth nanofilms[16] have been reported, however, no any intermediate state for silver thiolate based system has been observed, which may mainly due to the complex micellar phase formation for longer chain alkane thiolates at higher temperatures,[8] furthermore, the reactivity rate of the precursors has remarkable influence on the synthetic process of nanomaterials.[19]

By introducing azobenzene mesogen into silver thiolates, unusual lamellar liquid crystalline (LC) phases over a wide temperature range can be attained, which are quite different from those based on simple alkane metal thiolates under higher temperatures, such as micellar mesophases from silver alkane thiolates and hexagonal columnar phase from copper alkane thiolates.[2,8] Such persistent lamellar LC mesophases provide an opportunity for controlled preparation of metal or metal sulfide nanomaterials and investigating the mechanism of the layered-precusor-to-lamellar-nanoproduct of solventless thermolysis within a real constrained layered precursor system.

Herein in this paper, we introduce azobenzene mesogen for the first time into this organic-inorganic hybrid system to investigate the phase behavior of this novel series silver thiolates and the silver nanodisks preparation based on such mesogenic precursors. A series of thiols introducing azobenzene mesogen with different length alkoxy tail and thus their silver thiolates have been designed and synthesized, then a systematic study conducted on their thermal behavior and phase structures by differential scanning calorimetry (DSC), variable-temperature simultaneous small- and wide-angle X-ray scattering (SAXS/WAXS) and temperature dependent Fourier transform infrared spectroscopy (FTIR). Furthermore, two-dimensional (2D) disk-shaped silver nanomaterials preparation has been preliminarily explored based on the mesogenic silver thiolate precursors.

2. Experimental Section

2.1. Chemical reagents

Silver nitrate (99.8%), potassium thioacetate (98%) and sodium borohydride (98%) were purchased from Alfa Aesar and used as received without purification. Anhydrous tetrahydrofuran (THF) was distilled over sodium-benzophenone under nitrogen prior to use. All other chemical reagents were purified according to standard procedures before use.

2.2. Synthesis and characterization for the series silver thiolates 2

Synthesis of AgS-$C_{10}H_{21}$-Ph-N=N-Ph-OC_nH_{2n+1} with octyloxy tail of n = 8 (**2c**) is representatively shown here as an example, all other analogues were prepared by the same protocol using thiol ligands with variant tails. A solution of silver nitrate (17.0 mg, 0.1 mmol) in THF/H_2O (5 mL : 1 mL) mixture was added dropwisely into a solution of 4-(10-mercaptodecyl)-4'-octyloxy-azobenzene (**1c**, 150 mg, 0.3 mmol) in THF (15 mL) at room temperature. A light yellow precipitate was formed immediately, and the mixture was stirred for 2 h. The product was purified by washing with THF and ethanol for several times, then filtered and dried under vacuum overnight to produce solid powder in brown yellow of 60.3 mg at 91% yield. Anal. calcd. (%) for **2c**: C 59.50, H 7.49, N 4.63; found: C 60.14, H 7.93, N 4.24. Similarly, for **2a**: yield 93.6%, anal. calcd. (%) C 54.44, H 6.16, N 5.52; found: C 54.31, H 5.89, N 5.61; for **2b**: yield 91.8%, anal. calcd. (%) C 58.23, H 7.16, N 4.85; found: C 58.40, H 7.22, N 4.80; and for **2d**: yield 87.3%, anal. calcd. (%) C 60.65, H 7.79, N 4.42; found: C 61.54, H 7.92, N 4.21.

2.3. Instruments and measurements

^{1}H NMR spectra were obtained on 300 MHz (Bruker AMX300) instruments with TMS as internal standards. Mass spectra were recorded on a LCQ Fleet ion trap mass spectrometer by electrospray ionization. Elemental analyses (EA) were carried out with an Elementar Vario Micro. Fourier transform infrared spectra (FTIR) were recorded on a NICOLET NEXUS 870 infrared spectrometer equipped with a variable temperature control unit with a precision of ±1 °C using pressed potassium bromide pellet samples. Differential scanning calorimetry (DSC) traces were recorded on a Perkin-Elmer Pyris I calorimeter equipped with a cooling accessory with a 10 °C min^{-1} heating or cooling rate under a nitrogen atmosphere. Thermal gravimetric analysis (TGA) was performed using a Perkin-Elmer Pyris I instrument at a heating rate of 20 °C min^{-1} under a nitrogen atmosphere. Polarized optical microscopy (POM) texture investigation was conducted with melt-pressed samples sandwiched between two glass plates on a PM6000 optical microscope under cross-polarizers equipped with a Leitz-350 heating stage and an associated Nikon (D3100) digital camera. Variable-temperature X-ray scattering experiments were performed with a high-flux small-angle X-ray scattering instrument (SAXSess mc^2, Anton Paar) equipped with Kratky block-collimation system and a temperature control unit (Anton Paar TCS300). Both small-angle X-ray scattering (SAXS) and wide-angle X-ray scattering (WAXS) were simultaneously recorded on an imaging-plate (IP) which extended to high-angle range (the q range covered by the IP was from 0.06 to 29 nm^{-1}, $q = (4\pi\sin\theta)/\lambda$, where the wavelength λ is 0.1542 nm of Cu Kα radiation and 2θ is the scattering angle) at 40 kV and 50 mA for 5 min. Typically, the powder sample was encapsulated with aluminum foil during the measurement and the obtained X-ray analysis data were processed with the associated SAXSquant software 3.80. Transmission electron microscopy (TEM) studies were performed on a JEM-2100 (JEOL) at 200 kV. Each sample was prepared by depositing a drop of a dilute suspension of the corresponding nanocrystals in THF onto a carbon-film-coated Cu grid. For atomic force microscopy (AFM) investigation, the samples were prepared by drop-casting the dilute silver nanoparticles (nanodisks) suspension (0.1 mg/mL) onto a silicon substrate, after evaporation the AFM imaging and measurements were performed under ambient conditions using a JPK NanoWizard II system (JPK Instruments AG, Germany) working in tapping-mode (TM). The X-ray powder diffraction (XRD) patterns of inorganic samples were recorded on a Shimadzu XRD-6000 X-ray diffractometer by weighing about 10 mg of solid in a standard cavity mount with Cu Kα radiation at room temperature.

3. Results and Discussion

3.1 Synthesis

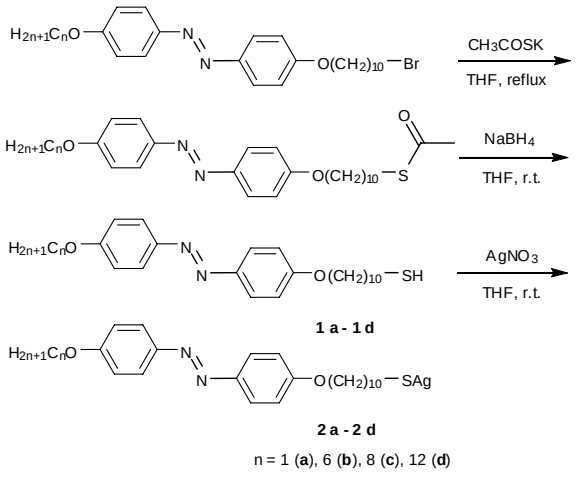

Scheme 1 Synthetic route of the series thiol ligands **1** and their corresponding silver thiolates **2**.

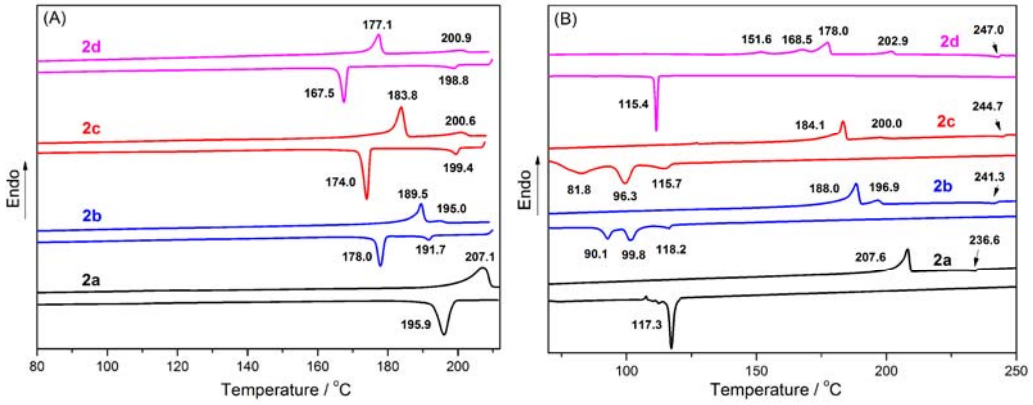

Fig. 1 DSC thermograms of the series silver thiolates **2a** - **2d** during (A) the 2nd heating and 1st cooling scans in the temperature range of 50-210 °C at a rate of 10 °C min^{-1}; and (B) the 1st heating and 1st cooling scans in the range of 50-250 °C at the same rate of 10 °C min^{-1}.

Table 1 Thermal properties and phase assignments for the thiol ligands **1** and corresponding silver thiolates **2** in the temperature range of 50–210 °C for the 1st cooling and 2nd heating runs.

code	T_{decomp} (°C)[a]	Thermal cycle	Transition T/℃ [ΔH (J g^{-1})][b,c]	LC range (°C)
1a	225	cooling	I 91.5 [71.5] Cr	/
		heating	Cr 101.4 [87.5] I	/
1b	232	cooling	I 99.1 [3.55] N 88.6 [3.26] SmA 66.9 [66.7] Cr	(10)+21
		heating	Cr 82.3 [87.5] SmA 91.4 [3.50] N 101.1 [3.3] I	9+(10)
1c	238	cooling	I 99.9 [1.98] N 97.6 [2.26] SmA 72.0 [74.8] Cr	(2)+26
		heating	Cr 82.9 [4.2] 94.9 [104.8] SmA 102.0 [12.7] I	7
1d	245	cooling	I 100.5 [14.8] SmA 82.3 [71.5] Cr	18
		heating	Cr 90.7 [75.0] SmA 103.4 [16.7] I	13
2a	333	cooling	I 195.9 [65.2] Cr	/
		heating	Cr 207.1 [88.6] I	/
2b	323	cooling	I 191.7 [8.4] SmX 177.9 [64.0] Cr	14
		heating	Cr 189.5 [56.4] SmX 195.0 [3.4] I	6
2c	330	cooling	I 199.4 [8.5] SmX 174.0 [62.0] Cr	25
		heating	Cr 183.8 [67.4] SmX 200.6 [9.8] I	17
2d	328	cooling	I 198.8 [7.4] SmX 167.5 [51.7] Cr	31
		heating	Cr 177.1 [78.9] SmX 200.9 [10.9] I	24

[a] The onset of decomposition temperatures determined from TGA at heating rate of 20 °C min^{-1} under a nitrogen atmosphere.
[b] The phase transition temperatures and enthalpy changes (in square brackets) obtained from DSC at 10°C min^{-1};
[c] Abbreviations: Cr = crystalline, SmA = smectic A, SmX = highly ordered smectic phase with unidentified intralamellar organization details, N = nematic, I = isotropic.

The synthetic route of the series azobenzene-containing thiol ligands 4-(10-mercaptodecyloxy)-4'-alkoxy-azobenzene (**1**) and their corresponding silver thiolates **2** are illustrated in Scheme 1. The detailed synthetic procedures for thiols **1** and characterization data by ^{1}H NMR, FTIR, and MS are provided in the ESI.† The preparations of silver thiolates **2** were according to a modified procedure of the literature method[20] as described in the experimental section.

3.2 Thermal properties and phase behaviors by DSC Measurements

Thermal properties of silver thiolates **2** and their corresponding thiol ligands **1** were first investigated by DSC and TGA. For the series thiolates **2**, it is interesting to note that when the highest temperature reached upon heating was low than the exothermic transition temperature around 245 °C, such as below 210 °C the DSC thermograms of heating and cooling cycles were almost

reversible as shown in panel A of Fig. 1, The thermal transition peak temperatures and associated enthalpy changes, also the phase assignments in combination with other characterization techniques as described next for silver thiolates **2** and their corresponding thiol ligands **1** (see Fig. S1 in the ESI†) are summarized in Table 1. While as shown in panel B of Fig. 1, when the maximum temperature in the first heating run reached 250 °C, which was beyond the temperature of phase transition peaks with a small exothermic enthalpy changes of 2-6 J g^{-1} at 237, 241, 245, and 247 °C for **2a** to **2d**, respectively, the thermogram traces in the cooling run were totally different with those curves displayed in Fig. 1A. Moreover, for all the series **2** samples after going through higher temperature 250 °C cycle, another almost reversible endothermic transitions lower than 150 °C were observed in the following heating runs and essentially reversible exothermic peaks exhibited in all succeeding cooling runs (see Fig. S2 and Table S1 in the ESI†). Such thermal behaviors were attributed to the thermolysis as indicated by the small exothermic peaks in the first heating run and after experiencing this *in situ* thermal reducing reaction, the sequential DSC traces displayed the thermal properties of corresponding thermolytic byproducts which will be confirmed in the next part to be mainly composed of azobenzene-containing alkyl sulfide and disulfide. It is worthy to note that thermolysis (thermal reduction) rather than decomposition occurred here as indicated by TGA analysis that for all the series **2** samples no detectable weight loss before 280 °C (Table 1, also see Fig. S3 in the ESI†).

As shown in Fig. 1A, before the thermolysis occurring, all thiolate samples exhibited enantiotropic mesophases except the silver thiolate **2a** with the shortest methoxy tail, the melting temperatures of the series silver thiolates decreased with the alkoxy tail length increasing from methoxy to dodecyloxy and showed about 10 °C supercooling in the cooling cycles, while the clearing temperatures increased from **2b** to **2d** thus leading to ever broadened liquid crystalline temperature range as listed in Table 1. The monotonically decreasing tendency of the melting temperatures of the azobenzene mesogen-containing series silver thiolates was in sharp contrast with the behavior of simple alkane silver thiolates ($AgSC_mH_{2m+1}$) which showed a chain-length independent almost unaltered melting temperature around 130 °C.[9] Based on the understanding that silver thiolates possess a bilayered structure as firstly proposed by Dance *et al*. with a rigid inorganic central slab through trigonal-planar coordination of Ag and three SR moieties, with the R groups extending almost perpendicular to both sides of the slab.[7] For the inorganic skeleton structure is not significantly perturbed by the organization of aliphatic alkyl chains originated from weaker van der Waals interactions, thus the melting temperature is almost unchanged for simple alkane thiolates $AgSC_mH_{2m+1}$ of variant alkyl length.[21] Whereas for the studied series thiolates **2a**-**2d**, owing to the introduction of mesogenic chromophore azobenzene exerting π-π interaction substantially stronger than van der Waals force, their melting points are obviously higher than those of aliphatic alkane thiolates and diminish with the decrease of proportion and extent of π-π stacking as alkoxy tail lengthening. Furthermore, it is interesting to notice that liquid crystalline mesophases, which will be confirmed to be highly ordered smectic phases by SAXS/WAXS analysis, POM investigation and temperature-dependent FTIR study as presented in the following context, were formed in the silver thiolates **2b**-**2d** derived from the mesogenic thiol ligands **1b**-**1d**, while no LC phase was observed in the thiolate **2a** originated from the crystalline thiol ligand **1a**.

3.3 Variable temperature SAXS/WAXS investigation

SAXS is a powerful tool and can often provide some structural details, simultaneous SAXS and WAXS investigations were performed *in situ* using a high-flux SAXSess X-ray scattering instrument equipped with a temperature control accessory for probing into the organized structure and phase characteristics of silver thiolates. As representatively shown in Fig. 2 for **2c**, all the series thiolates investigated displayed layered structures in their crystalline solid with more than ten orders reflection fringes in the low-angle region and lamellar mesophases with five equidistant SAXS peaks after melting for **2b** to **2d** with longer alkoxy tails (Fig. 2A and also see Fig. S4 in the ESI†). The background peaks from the packing aluminum foil as marked by an asterisk locating in the wide-angle region have a negligible disturbance to the interested sample peaks, thus no complete subtraction was conducted so as to avoid distortion of the peak shape and smoothing over some significant weak signals. Furthermore, with the introduction of mesogenic azobenzene, besides the SAXS higher order reflections of lamellar structure, three characteristic reflections in the WAXS region exhibited in the crystalline state, the band at around 14.80 nm^{-1} (0.42 nm distance) superimposed by some weak higher order peaks of the layered structure was attributed to average alkyl interchain spacing due to van der Waals interaction (Fig. 2A). As shown in Fig. 2B, another two peaks with q values of 17.20 and 21.15 nm^{-1} (corresponding to 0.37 and 0.30 nm, respectively), were ascribed to azobenzene moiety of π-π stacking and the intralayer structure of Ag-S slab, respectively,[7,9,21] their temperature dependent shifts were discussed later in this paper. Upon heating into the mesophase state as at 190 °C, with disappearance of crystalline fringes five new reflections appeared in the small-angle range with q ratio of 1:2:3:4:5 characterizing a highly ordered lamellar liquid crystalline mesophase of spacing 5.51 nm, which was 1.24 nm shorter than the 6.75 nm observed in the crystalline state implying tilt or disorder of melted alkyl chains as demonstrated by the following temperature-dependent FTIR investigation. Highly ordered smectic like thin films from azobenzenes showing up to eight Bragg reflections were reported by the thermal evaporation method or Langmuir-Blodgett (LB) technique.[22] Moreover, a shoulder reflection of lower intensity as indicated by an arrow emerged, and as temperature further increased to such as 210 °C two broad reflections appeared at q = 1.35 and 2.80 nm^{-1} presumably attributed to the mixture of residual lamellar structure of precursor and the silver nanoparticles formed due to partial thermolysis within the time period of measurement at high temperature which will be further discussed in the following context. Similar to **2c**, **2b** and **2d** also exhibited lamellar mesophases, while with methoxy tail **2a** directly melted into isotropic state in agreement with DSC analysis results. The interlayer spacings of **2b** and **2d** in their mesophases were shortened to 5.34, 6.10 nm compared with 6.28 and 7.66 nm in

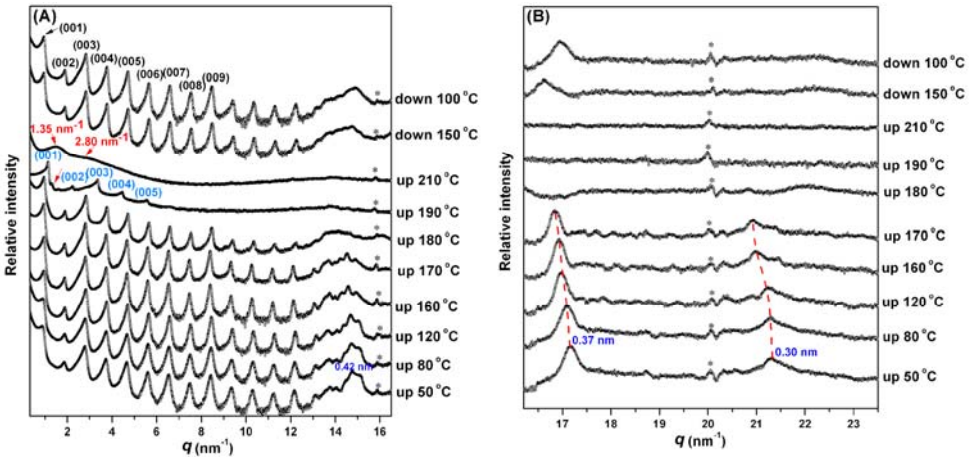

Fig. 2 SAXS/WAXS profiles of silver thiolate **2c** at variant temperatures upon heating up or cooling down cycles: (A) q = 0.32-16.5 nm^{-1}; (B) q = 16.0-24 nm^{-1}. The peaks labeled by asterisks are due to reflections of the packing aluminum foil background.

their corresponding crystalline phases, respectively. The dependence of the interlayer spacing d against the alkoxy tail carbon number n in the crystalline phase obeyed strictly linear relationship of d = 4.96 + 0.22 n (with correlation coefficient R^2 = 0.999, see Fig. S5 in the ESI †), which was similar to the trendline of simple alkane silver thiolates with a much larger intercept value of 4.96 nm compared with ~0.8 nm[23] due to the contribution of azobenzene and decyloxy spacer.

3.4 Texture observation by POM

The phase transition and mesomorphic properties of the silver thiolates together with their corresponding thiol ligands were further confirmed by polarizing optical microscopy (POM) investigation. As representatively shown in Fig. 3a and b for ligand **1b**, typical focal conical texture of smectic A phase (SmA) and schlieren texture of nematic phase (N) were observed largely in agreement with the temperature ranges determined by DSC for thiol ligands **1b** to **1d** (Table 1, also see Fig. S1 and S6 in the ESI †), which were also confirmed by the SAXS/WAXS study (see Fig. S7 in the ESI†). For silver thiolate **2a**, only spherulitic crystalline texture observed upon cooling from isotropic phase corroborated its crystalline character without any mesophase formation (Fig. 3c). It is interesting that for the longer tail mesogenic silver thiolates, **2b** showed mosaic like texture with some extinction area (Fig. 3d), the texture of **2c** was quite similar to that of **2b** with some small focal conical patterns superimposed (Fig. 3e), and **2d** exhibited pseudo focal conical texture (Fig. 3f), all these textures could be attributed to some kind of highly ordered smectic phases,[24-27] while they might also be displayed by some typical columnar mesophases as generated from discotic mesogens.[28,29] Therefore, here attention is prompted to avoid a columnar phase misjudgment just based on POM textures, in fact from the temperature-dependent SAXS profiles as discussed above showing more than four order reflections, in combination with their thermal properties and POM observations, the LC mesophases can be assigned affirmatively to be some kind of highly ordered smectic phase SmX, which is also quite reasonable as a successive mesophase derived from the orthorhombic crystalline precursor phase as demonstrated next by the temperature dependent FTIR investigation, while at the moment we cannot determine their detailed intralamellar arrangement due to the lack of sufficient signals to characterize the lateral structure within the lamellar.

3.5 Temperature dependent FTIR study

Fourier transform infrared spectroscopy (FTIR) can provide a highly sensitive probe of molecular structure and dynamics of alkyl chains,[23,30,31] thus variable-temperature FTIR was employed to explore the silver thiolates for better understanding their phase structure and transition at molecular level. As representatively shown in Fig. 4 for **2c**, 2954 and 2873 cm^{-1} vibrations were assigned to asymmetric (r^-) and symmetric (r^+) stretching vibrations of the terminal methyl groups, respectively. A remarkable shoulder at 2935 cm^{-1} was attributed to the Fermi resonances of the zigzag conformer of the polymethylene chain (r^+_{FR}).[23,31] The r^- and r^+ bands of the terminal methyl groups became diminished and gradually difficult to identify from the second to third phase transition (Fig. 4a). The stronger bands at 2918 and 2849 cm^{-1} were assigned to asymmetric (d^-) and symmetric (d^+) stretching vibrations of the methylene group, respectively. The d^- and d^+ ranges are known to be a strong indicator of chain conformation with low wavenumbers 2916-2918 and 2846-2849 cm^{-1} characteristic of the ordered all-trans extended alkane chains, and upward shifting to 2924-2928 and 2854-2856 cm^{-1} indicative of the significant increase in gauche population or switching to high-temperature liquid-like disorder state.[23,30] Based on this cognition, the observed peak frequencies of 2919 and 2849 cm^{-1} before melting indicated the predominantly all-trans crystalline state, while obviously shifting to higher wavenumbers and peak broadening exhibited when the temperature was increased to around 170 °C (Fig. 4a), slightly lower than the melting transition temperature determined by DSC measurements, indicating increased disorder of the alkyl chain ensembles and a pre-melting transition to some extent.[23,30] The peaks became much broader when entering the isotropic amorphous phase, all these spectral behaviors were quite similar

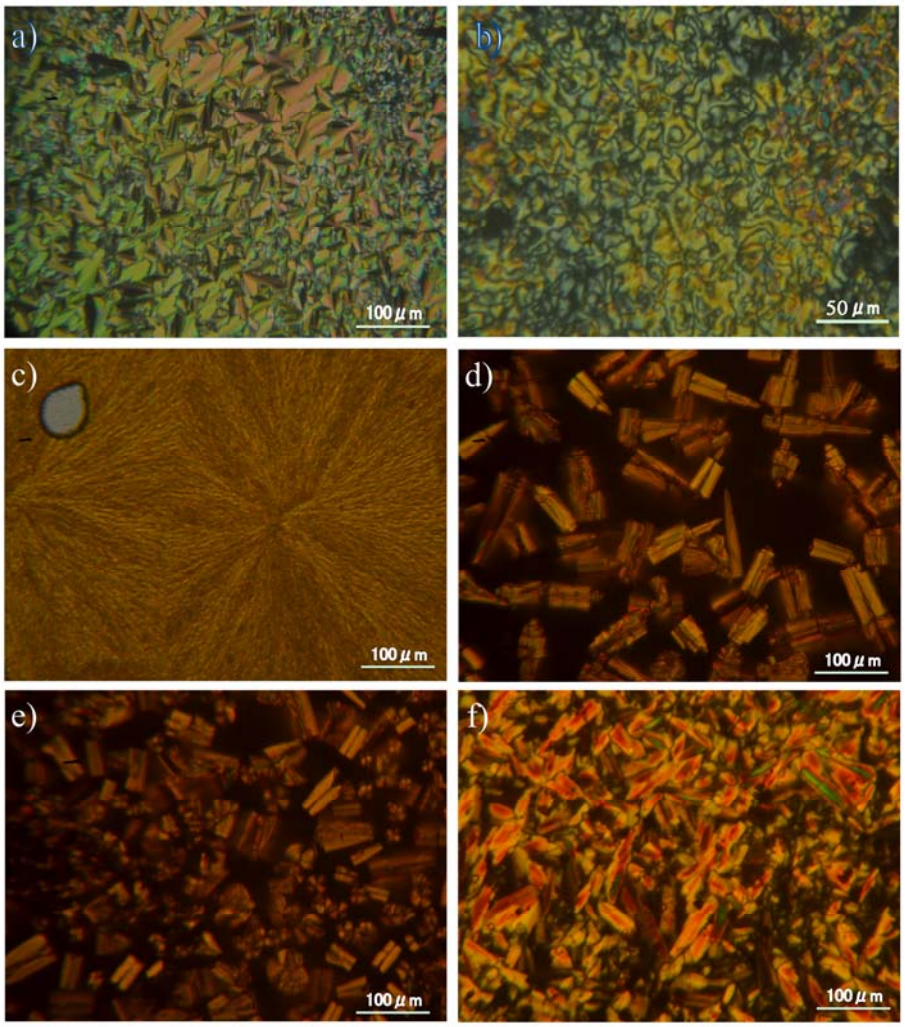

Fig. 3 Representative POM texture images under crossed polarizers of silver thiolates and a typical thiol ligand: (a) ligand **1b** at 85 °C, SmA; (b) **1b** at 98 °C, N; (c) thiolate **2a** at 193 °C, Cr; (d) **2b** at 191 °C; (e) **2c** at 188 °C; and (f) **2d** at 190 °C, SmX.

to that of the simple alkane silver thiolates.[23,30] Some more specific characters exhibited in the lower frequency region for the mesogenic silver thiolates were examined. The characteristic vibrational peaks located at 1602, 1581, and 1498 cm^{-1} were from the aromatic ring, and the strong bands at 1247 cm^{-1} and 1150 cm^{-1} were due to the phenyl ring-O vibration and phenyl-N stretching mode, respectively.[31] The vibrational band assigned to phenyl ring was more sensitive and became broader accompanied with a downward shifting from 1603 to 1599 cm^{-1} as the temperature only rose to around 160 °C, followed by broadening and further shifted to 1597 cm^{-1} as the temperature passed through the second to third phase transition (Fig. 4b). The most interested spectral indications for the current examined azobenzene based thiolate system were revealed by some characteristic low frequency bands. The bands within the range of 1465 to 1473 cm^{-1} corresponding to CH_2 scissoring bending modes are widely used to diagnose alkyl chains packing, the occurrence of a single narrow peak at 1473 cm^{-1} is ascribed to triclinic subcell packing of alkyl chains, while a single band at 1467 cm^{-1} indicates a hexagonal subcell, both subcells are the crystal ones of a single chain in an individual cell.[23,30,31] In the present case, the slightly split peaks at 1473 and 1465 cm^{-1} (Fig. 4b) were presumably derived from orthorhombic arrangements of the alkyl tail chains by interchain interactions between the contiguous CH_2 groups of the two chains constituting the crystal sub-cell.[23,32] This kind of splitting, referred to as factor-group splitting, is specific to orthorhombic sub-cells.[23] Upon heating to above 170°C the split bands at 1473 and 1465 cm^{-1} merged into a single wider band at 1467 cm^{-1}. Moreover, as shown in Fig. 4c and 4d in the crystalline solid state below 160 °C, the split bands at 1394 and 1385 cm^{-1} assigned to the CH_3 symmetric deformation or bending vibration, the slightly split bands at 1026 and 1016 cm^{-1} attributed to the skeletal modes of the hydrocarbon chains or C-C-C backbone stretching modes, and the spilt bands at 721 and 730 cm^{-1} assigned to the methylene C-H rocking mode, which are all very sensitive to the environment and to interlamellar interactions, further confirmed the orthorhombic packing feature.[23,30] This highly ordered orthorhombic organization is in sharp contrast to the usually hexagonal packing structure observed in simple alkane silver thiolate[23,30] or to the

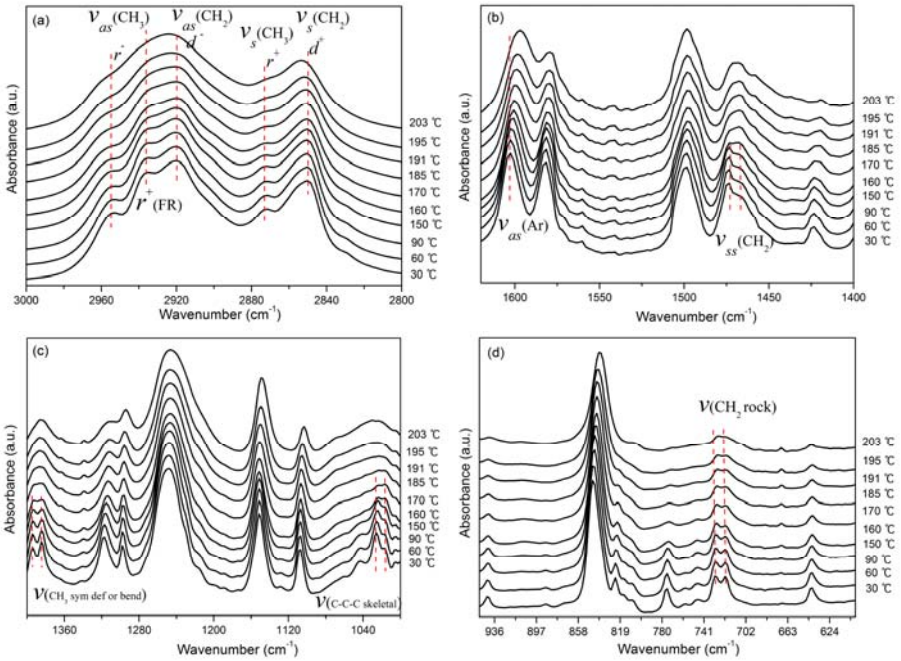

Fig. 4 Variable-temperature FTIR spectra of **2c** over the temperature range 30-203 °C at (a) high-frequency region (3000-2800 cm^{-1}); and low-frequency region: (b) 1650-1400 cm^{-1}; (c) 1400-1000 cm^{-1}; and (d) 950-600 cm^{-1}.

mainly hexagonal or mixed arrangements exhibited in the complex clusters of azobenzene-based cationic surfactants and polyoxometalates,[31] which is ascribed to both the stronger π-π stacking interactions introduced by azobenzene mesogenic units and the skeleton binding of the inorganic Ag-S slab as will be illustrated later in this paper.

3.6 2D shaped Ag nanodisks preparation through thermolysis within or near the lamellar LC mesophases

Based on some reflections other than the layered crystalline fringes Dance *et al*. proposed a general lattice geometry for some short chain alkyl and *para*-substituted phenyl silver thiolates.[7] Though no suitable thiolate single crystals were available for full analysis of the two dimensional intralamellar organization, the shifts of diffraction peak at around q = 21.15 nm^{-1} (0.30 nm, labeled by a red dashed line for guide the eye in Fig. 2b) characteristic of the Ag-S inorganic slab were indicative of the structure adjustment or coordination symmetry change with temperature especially around phase transition. As shown in Fig. 2b, the diffraction peak shifted to lower angle at temperature higher than 120 °C and disappeared at around 180 °C approaching the mesophase transition temperature, which was due to elongation or fracture of some Ag-S connection inside the inorganic slab upon heating resulting in the coordination symmetry change from regular trigonal planar structure in the crystalline state to a mixture of digonal and trigonal coordination at higher temperature as observed in the alkane silver thiolates.[7] It was worthy to note that the reflections characteristic of the main layered structure such as the crystalline fringes due to self-assemble of alkyl chain and π-π stacking of azobenzene were essentially reversible upon cooling from their mesophases, while the diffraction pattern due to Ag-S inorganic slab was largely irreversible, especially when the silver thiolates were held at higher temperature for a prolonged time. Such as for dodecyloxy tail thiolate **2d**, which also showed a weak shoulder superimposed on the (001) peak besides the multiple evenly spaced reflections of up to six orders at a normal measuring run upon heating to 190 °C indicating a mesophase lamellar structure similar to that of **2c** (Fig. 2A), while an obviously enhanced scattering peak at 1.30 nm^{-1} with q slightly downward shifted lamellar structure reflections exhibited after isothermal annealing for 30 minutes at 190 °C (see Fig. S8 in the ESI†). Such SAXS signal evolution could be reasonably interpreted as the changes of size and morphology of intermediate thiol capped silver nanoparticles reduced from the thiolate precursors as will be demonstrated in the following paragraphs from **2c**-based system for example, which implied that for the mesogenic silver thiolates (**2b-2d**) the process of thermolysis could be triggered in the temperature range of LC mesophases in sharp contrast to the suggested reversible rearrangement of μ^3-bridged solid structure into a cyclic μ^2-bridged micellar mesophase structure reported for simple alkane thiolates $AgSC_mH_{2m+1}$.[8]

Solventless thermolysis is an environmentally friendly and intriguing method in synthesis of various metal or metal sulfide nanomaterials from their metal thiolate precursors.[11-18] The structure and composition of the precursors played a crucial role in determining the size and morphology of thus produced reducing nanoproducts.[19] Wu *et al.* reported an example of Ag nanodisks preparation from long chain alkane thiolate $AgSC_mH_{2m+1}$ under certain carefully controlled conditions, and they proposed a layered-precursor-to-lamellar-nanoproduct mechanism for the size and shape controlling of thus produced nanomaterials.[18] While for simple alkane thiolate precursors the layered structure cannot be preserved under temperature just a little higher than their melting points due to the complex phase

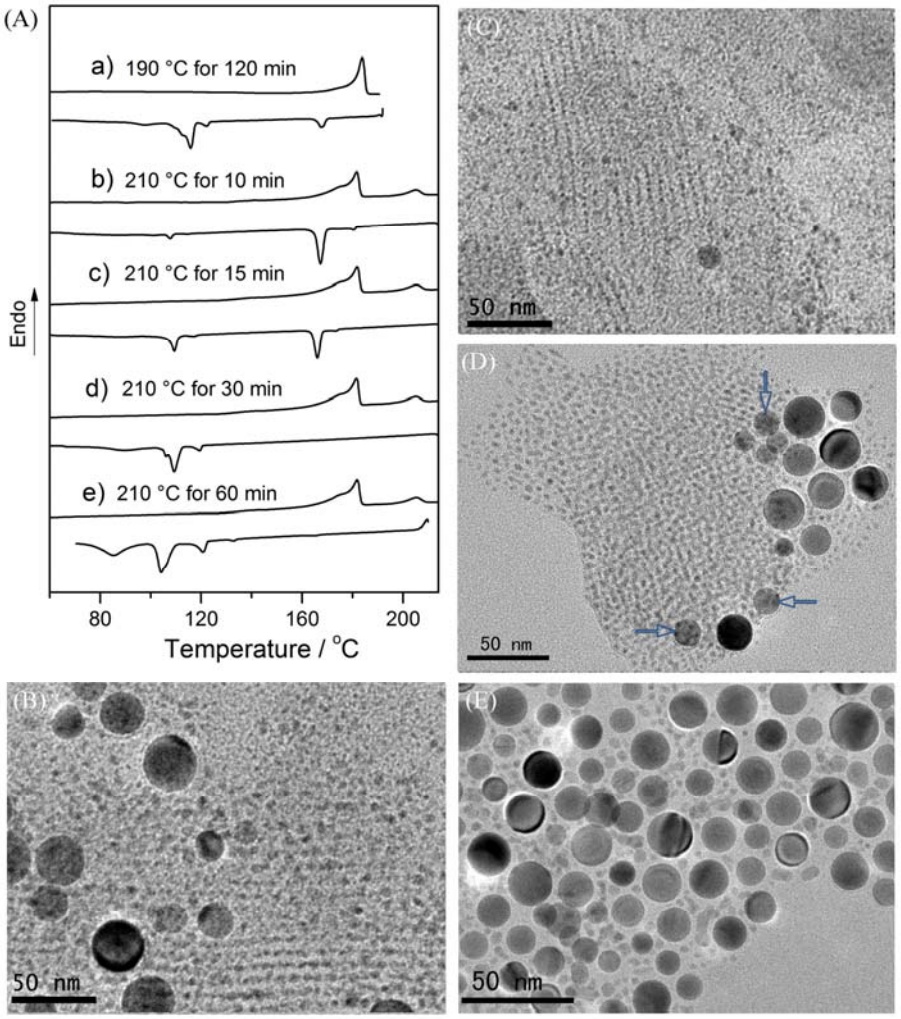

Fig. 5 (A) DSC thermograms of **2c** experiencing different thermal history a) heating to 190 °C and isothermal annealing for 2 h then cooling; b-e) first heating to 210 °C and isothermally annealing for 10, 15, 30, and 60 min then cooling, respectively, with all heating and cooling scans at the same rate of 10 °C min^{-1}. TEM micrographs of Ag nanoproducts produced from **2c** after the *in situ* thermolytic reaction as accordingly described in panel A after DSC thermal cycles a, c, d, and e of annealing at 190 °C for 2h (B) or 210 °C for 15 min (C), 30 min (D), and 60 min (E), respectively.

evolution,[8] so reproducible production of certain shaped nanomaterials is not easy to realize and no any intermediates supporting the suggested mechanism have ever been observed due to their rather high reaction rate. In the investigated **2** series thiolates, the SAXS/WAXS analysis results implied that the triggering times of Ag nanoparticles formation at the high temperature end of mesophase ranges were different for variant analogues (Fig. 2, also see Fig. S4 and S8 in the ESI†), which were consistent with their instability performance as indicated by DSC measurements (Fig. 1, and see Fig. S2 in the ESI†). The thiolates showing LC mesophases exhibited more stable during the repetitive heating cycles or isothermal annealing compared with **2a** (Fig. S9 in the ESI†). A mixture state of undissociated lamellar structure and reduced silver nanoparticles coexisted for LC thiolates **2b - 2d**, while crystalline **2a** quickly reached almost completion of thermolysis which implied controllable much slower thermolytic reaction rates for the LC thiolates compared with non-LC analogues such as **2a** and in particular the simple alkane silver thiolates $AgSC_mH_{2m+1}$.

3.7 LPLM thermolytic reaction mechanism

The much lowered reaction rate in the LC thiolate system offered an opportunity to monitor the reaction process during thermolysis and better understand the reaction mechanism. More important, the persistent real layered mesophases may provide an ideal confined environment according to a layered-precursor-to-lamellar-nanomaterial (LPLM) thermolysis pathway to prepare 2D constrained nanoproducts. Taking **2c** as an example**,** based on a batch of comparison experiments loaded with similar amount of reagents, the effects of thermolysis reaction temperature and time on the product size and morphology were investigated by DSC and TEM. Here DSC served as a sensitive and very effective method to monitor the thermolytic reaction progress, although as discussed previously that essentially almost reversible thermal behavior exhibited for the **2** series samples in the normal thermal

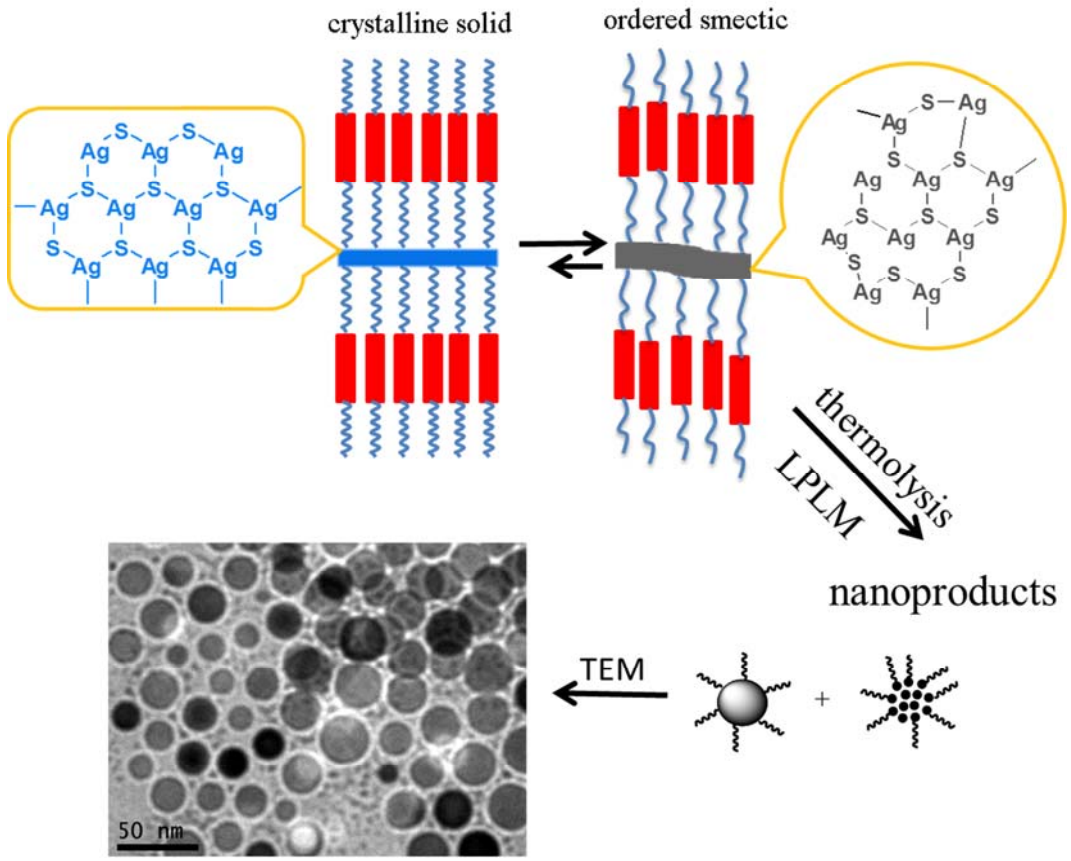

Fig. 6 Schematic representation of the proposed structures of azobenzene-based silver thiolates in crystalline solid state and the ordered smectic liquid crystalline mesophase, and the formation of intermediate nanoparticle aggregates and controlled preparation of 2D disk-shaped nanoproducts imaged by TEM from thermolytic reaction through a layered-precursor-to-lamellar-nanomaterial (LPLM) mechanism (with insets showing the suggested coordination change from regular trigonal planar symmetry in the crystalline state to the mixture of digonal and trigonal coordination due to partial thermolysis inside the inorganic Ag-S slab in the smectic phase).

cycles below 210 °C, obvious thermolysis occurred when annealing in their LC mesophases for a prolonged time such as isothermal annealing at 190 °C for 2 h resulted in most thermolytic products (thermogram curves group a in Fig. 5A), which was further confirmed by the direct TEM observation of resulted products showing some Ag nanodisks and nanoparticles with diameter ≤ 6.0 nm (Fig. 5B).

When isothermal annealing was conducted at a higher temperature just above the LC clearing temperature with some residual order as revealed by temperature dependent SAXS and FTIR studies, such as 210 °C for **2c** as shown in Fig. 5A, much remarkable thermolysis took place within shorter reaction time 10-60 min, even no peak detected for precursor silver thiolate at around 167 °C in the cooling scan only after 30 min isothermal annealing indicating almost completion of the thermolytic reaction into reduced products. The reaction evolution was also verified by TEM investigation directly. As shown in Fig. 5C, nanoparticles were mainly obtained with somewhat regular alignment by annealing for 15 min at 210 °C (average diameter less than 3.0 nm). After annealing for 30 min, the nanoparticles became bigger obviously, and a nice bit of nanodisks emerged, with some disks showing obvious nanoparticles aggregation as labeled by arrows indicated strongly that the nanodisks were formed by the fusion of nanoparticles (Fig. 5D). As the annealing time extended to 1 h, most of the small particles conglomerate into quite uniform nanodisks with an average diameter of 22.6 ± 2.2 nm, (Fig. 5E, also see Fig. S10 in the ESI†). AFM can offer sub-nanometer precision in height measurements,[33] the measured heights of nanodisks by AFM were around 2 ~ 4 nm (see Fig. S11 in the ESI†), which were slightly larger than the disk thickness reported from alkane silver thiolate precursor by Wu and co-workers[18] and presumably due to the longer azobenzene mesogenic capping agents and without optimization of experimental conditions for materials preparation. The much diminished and controllable reaction rate of the LC silver thiolates facilitated the first observation of the intermediate nanoparticles in this kind of system in contrast with that of $AgSC_mH_{2m+1}$.

XRD analysis confirmed the fcc character of thus produced silver nanodisks (as compared with standard fcc Ag pattern JCPDS 4-783, see Fig. S12 in the ESI†). Furthermore, the silver nanoproducts were validated to be capped with the azobenzene thiol ligands by FTIR and energy dispersive X-ray (EDX) analyses. The main characteristic peaks such as 2919 and 2849 cm^{-1} of methylene stretching vibrations, 1603 and 1581 cm^{-1} of typical vibration absorption of benzene ring, and 1247 cm^{-1} and

1150 cm^{-1} of the phenyl ring-O vibration and phenyl-N stretching mode were clearly observed in the FTIR spectrum of reduced Ag nanoproduct (Fig. S13a in the ESI†). Its EDX profile indicated that the S, O and N elements co-existing with Ag (Fig. S13b in the ESI†) thus also proved the character of azobenzene thiol capped Ag nanoproduct. For better understanding the thermolysis process, the byproducts of the thermolytic reaction were also briefly analyzed using ^{1}H NMR in comparison with correspondingly synthesized alkyl disulfide samples and literature results.[5] The double triplet peaks at around 2.7 and 2.5 ppm of the ^{1}H NMR spectrum characteristic of the methylene protons adjacent to sulfur in disulfide -CH_2-S-S-CH_2- (Fig. S14A in the ESI†) and sulfide -C*H*$_2$-S-C*H*$_2$-, respectively, rather than the quartet peak of alkyl thiol (Fig. S14B in the ESI†) verified the presence of both disulfide and sulfide in the byproducts.[5] So the thermolytic reaction was suggested as schematically showing below:

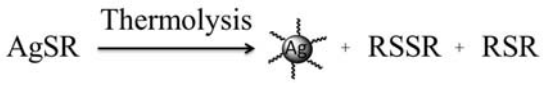

where **R**: -$C_{10}H_{21}$-Ph-N=N-Ph-OC_nH_{2n+1}, n = 1, 6, 8, 12

For other mesogenic thiolates examined such as **2b** and **2d**, their phase behaviors and reduced nanoproducts were quite similar to that of **2c**, nanoparticles were first formed and conglomerated into 2D nanodisks slowly. While for the thiolate without LC mesophase as **2a**, a much quick formation of relative irregular nanoproducts was observed due to the rapid thermolytic reaction (Fig. S15 in the ESI†). The DSC investigation and the direct TEM observation of thus produced nanoproducts combining with spectral characterization and byproducts analysis, help one to better understand the thermolytic reaction process and phase transition and to elucidate the LPLM mechanism. Mainly small Ag nanoparticles were produced under relatively low temperature or short reaction time such as for **2c** annealing at 210 °C for 10 min, then the small nanoparticles restrained by the layered structure of the precusor aggregated and merged into nanodisks during the subsequent thermal reaction. The growth in thickness direction constrained and hindered by the long organic chain bilayers was much slower than in diameter dimension controlled by intralamellar diffusion. By the way, the thermolytic reaction performance of series **2** samples at high temperature 250 °C above their exothermic transitions far from the LC clearing points may also serve as a circumstantial evidence for the constraint character within or very near the LC mesophases. Mainly three dimensional Ag nanospheres of monotonically decreased size from 59.3 ± 2.7 nm for **2a** to 16.1 ± 1.4 nm for **2d** with the increased alkoxy tail lengths were obtained under 250 °C thermolysis, demonstrating the almost loss of 2D restraint at high temperature and another alternative control mechanism taking effect principally on volume ratio of reactive inorganic moieties to nonpolar hydrocarbon matrix as will be reported elsewhere in details.

The suggested structures of azobenzene-based silver thiolates in their crystalline solid and the lamellar liquid crystalline mesophase, also the intermediate nanoparticle aggregates and disk-shaped nanoproducts from thermolytic reaction imaged by TEM have been schematically depicted in Fig. 6. Herein, as sketched in the insets we speculated that the inorganic skeleton of Ag-S still maintained as a relatively incompact stratum though experiencing bond changes from strictly regular trigonal symmetry into a structure of partial elongation or fracture of Ag-S connection as proposed in the simple alkane silver thiolate system.[7] The adoption of azobenzene mesogenic ligands led to the silver thiolates with quite broad range of ordered lamellar LC mesophases due to the cooperativity between π-π stacking of azobenzene mesogen and the inorganic framework of Ag-S slab, which provided an ideal 2D confined environment to explore the thermolytic reaction mechanism and prepare 2D shaped nanomaterials through solventless thermolysis.

Herein the mesogenic ligands are not limited to azobenzene chromophore and the thermal reduced nanoproducts not circumscribed to silver, other systems based on such as biphenyl mesogenic unit and metal chalcogenide nanomaterials, e.g. cuprous sulfide ultrathin nanoribbons and nanofilms have been similarly prepared in our lab with excellent controllability and will be reported separately soon. The silver thiolates with mesogenic ligands are a kind of metal-containing liquid crystals and belong to the well-known metallomesogens, which combine the intrinsic characteristics of liquid crystals with the unique properties associated with metal atoms.[34] While unlike the usually reported metallomesogens focusing on the study of structure and phase behavior after introducing different metals and their comparison with the precursor liquid crystals without metal,[35] the silver mesogenic thiolates mainly serve as a kind of functional metallomesogen precursors with LC mesophases to provide the constrained environment for the controlled preparation of variant nanomaterials, especially the persistent ordered lamellar mesophases provide an intrinsic 2D restrained space for the facile controllable production of 2D shaped nanomaterials rather than the dependence on fine control of preparation conditions from the system based on simple alkane silver thilate precursors.

4. Conclusions

In summary, a series of azobenzene-containing thiol ligands with different length alkoxy tails and their corresponding silver thiolates have been successfully synthesized, then their thermal properties and phase behavior have been systematically investigated using thermal analysis and multiple variable-temperature characterization techniques, furthermore, based on the mesogenic silver thiolate precursors the preparation of 2D shaped silver nanodisks has been demonstrated in principle.

By introducing azobenzene mesogen for the first time into the silver thiolates, the organic-inorganic hybrid complexes **2b** to **2d** exhibited highly ordered smectic mesophases at obviously higher temperatures derived from the orthorhombic crystalline structure as elucidated by combination of the temperature dependent FTIR, POM and SAXS/WAXS investigations, which was attributed to the cooperativity between azobenzene π-π stacking and the skeleton binding of inorganic Ag-S slab, and led to their intriguing good performance compared with silver alkane thiolates or some other azobenzene chromophore based complex systems without the binding slab.

As a kind of functional metallomesogen precursor the silver mesogenic thiolates with persistent ordered lamellar LC

mesophases provide an ideal 2D confined environment for the investigation of LPLM mechanism of solventless thermolysis and may intrinsically stimulate the controlled preparation of variant 2D shaped metal and metal sulfide nanomaterials.

Acknowledgements

This work was supported by the National Natural Science Foundation of China (NSFC20874044) and Fundamental Research Plan Project of Jiangsu Province (BK2010244) and also partially by the National Science Fund for Talent Training in Basic Science (No.J1103310). We also thank Prof. Yi Cao of Physics School of Nanjing University for the assistance with AFM measurements.

Notes and references

[a] *Department of Polymer Science and Engineering, Key Laboratory of Mesoscopic Chemistry of Ministry of Education, School of Chemistry and Chemical Engineering, Nanjing University, Nanjing 210093, P. R. China. Fax: (+86)25-8331-7761. E-mail: cdz@nju.edu.cn*
[b] *Center for Materials Analysis, Nanjing University, Nanjing, 210093, P. R. China*
[c] *Department of Physics and Electronic Science, Changsha University of Science and Technology, Changsha, Hunan 410076, P. R. China*

† Electronic Supplementary Information (ESI) available: [Experimental procedures, synthesis and characterization for thiol ligands and some intermediates; DSC, POM and XRD characterization for thiol ligands **1a-1d**; TGA thermograms of thiolates **2a-2d**, and some additional DSC curves and variable-temperature SAXS/WAXS profiles for **2a**, **2b** and **2d**; FTIR, EDX and XRD profiles of produced silver nanomaterials; NMR analysis of thermolytic reaction byproducts compared to thiol ligand and disulfide; AFM images and additional TEM micrographs]. See DOI: 10.1039/b000000x/

1 (a) I. G. Dance, *Polyhedron*, 1986, **5**, 1037-1104; (b) D. W. Stephan and T. T. Nadasdi, *Coordination Chemistry Reviews*, 1996, **147**, 147-208.
2 P. Espinet, M. C. Lequerica and J. M. Martin-Alvarez, *Chem. Eur. J.*, 1999, **5**, 1982-1986.
3 N. Sandhyarani and T. Pradeep, *J. Mater. Chem.*, 2001, **11**, 1294-1299.
4 S. H. Cha, J. U. Kim, K. H. Kim and J. C. Lee, *Chem. Mater.*, 2007, **19**, 6297-6303.
5 S. H. Cha, K. H. Kim, J. U. Kim, W. K. Lee and J. C. Lee, *J. Phys. Chem. C*, 2008, **112**, 13862-13868.
6 Y. X. Zhang and H. C. Zeng, *Adv. Mater.*, 2009, **21**, 4962–4965.
7 I. G. Dance, K. J. Fisher, R. M. H. Banda and M. L. Scudder, *Inorg. Chem.*, 1991, **30**, 183-187.
8 M. J. Baena, P. Espinet, M. C. Lequerica and A. M. Levelut, *J. Am. Chem. Soc.*, 1992, **114**, 4182–4185.
9 A. A. Levchenko, C. K. Yee, A. N. Parikh and A. Navrotsky, *Chem. Mater.*, 2005, **17**, 5428-5438.
10 (a) Z. B. Zhang, X. T. Lu, Q. Peng and Y. D. Li, *Chem. Eur. J.*, 2011, **17**, 10445 – 10452; (b) Y. Wang, Y. X. Hu, Q. Zhang, J. P. Ge, Z. D. Lu, Y. B. Hou and Y. D. Yin, *Inorg. Chem.*, 2010, **49**, 6601 – 6608.
11 T. H. Larsen, M. Sigman, A. R. Ghezelbash, C. Doty and B. A. Korgel, *J. Am. Chem. Soc.*, 2003, **125**, 5638-5639.
12 M. B. Sigman, Jr., A. Ghezelbash, T. Hanrath, A. E. Saunders, F. Lee and B. A. Korgel, *J. Am. Chem. Soc.*, 2003, **125**, 16050 – 16057.
13 A. Ghezelbash, M. Sigman, Jr. and B. A. Korgel, *Nano lett.*, 2004, **4**, 537-542.
14 M. Sigman, Jr. and B. A. Korgel, *Chem. Mater.*, 2005, **17**, 1655-1660.
15 (a) L. Chen, Y. B. Chen and L. M. Wu, *J. Am. Chem. Soc.*, 2004, **126**, 16334 – 16335; (b) Y. B. Chen, L. Chen and L. M. Wu, *Chem. Eur. J.*, 2008, **14**, 11069 – 11075.
16 J. Chen, L. M. Wu and L. Chen, *Inorg. Chem.*, 2007, **46**, 586-591.
17 J. Chen, L. Chen and L. M. Wu, *Inorg. Chem.*, 2007, **46**, 8038 – 8043.
18 Y. B. Chen, L. Chen and L. M. Wu, *Inorg. Chem.*, 2005, **44**, 9817 – 9822.
19 K. L. Sowers, B. Swartz and T. D Krauss, *Chem. Mater.*, 2013, **25**, 1351−1362.
20 R. Voicu, A. Badia, F. Morin, R. B. Lennox and T. H. Ellis, *Chem. Mater.*, 2000, **12**, 2646- 2652.
21 H. G. Fijolek, J. R. Grohal, J. L. Sample and M. J. Natan, *Inorg. Chem.*, 1997, **36**, 622–628.
22 R. Jones, R. H. Tredgold, Z. Ali-Adib, A. P. L. Dawes, *Thin Solid Films*, 1991, **200**, 375 – 384.
23 A. N. Parikh, S. D. Gillmor, J. D. Beers, K. M. Beardmore, R. W. Cutts and B. I. Swanson, *J. Phys. Chem. B*, 1999, **103**, 2850–2861.
24 G. W. Gray and J. W. Goodby, *Smectic Liquid Crystals-Textures and Structures*, Leonard Hill, London, 1984, pp. 35-43.
25 P. K. Lo, D. Z. Chen, Q. W. Meng and M. S. Wong, *Chem. Mater.*, 2006, **18**, 3924-3930.
26 Q. W. Meng, X. H. Sun, Z. Y. Lu, P. F. Xia, Z. H. Shi, D. Z. Chen, M. S. Wong, S. Wakim, J. P. Lu, J. M. Baribeau and Y. Tao, *Chem. Eur. J.*, 2009, **15**, 3474-3487.
27 Z. H. Shi, D. Z. Chen, H. J. Lu, B. Wu, J. Ma, R. S. Cheng, J. L. Fang and X. F. Chen, *Soft Matter*, 2012, **8**, 6174-6184.
28 S. Kumar, *Chemistry of Discotic Liquid Crystals: From Monomers to Polymers* (Percec V. ed. The Liquid Crystals Book Series), CRC Press, Tayor & Francis Group, Boca Raton, 2011.
29 B. Wu, B. Mu, S. Wang, J. F. Duan, J. L. Fang, R. S. Cheng and D. Z. Chen, *Macromolecules*, 2013, **46**, 2916–2929.
30 J. F. Bardeau, A. N. Parikh, J. D. Beers and B. I. Swanson, *J. Phys. Chem. B*, 2000, **104**, 627–635.
31 W. Li, S. Y. Yi, Y. Q. Wu and L. X. Wu, *J. Phys. Chem. B*, 2006, **110**, 16961-16966.
32 H. L. Casal, H. H. Mantsch and D. G. Cameron, *J. Chem. Phys.*, 1982, **77**, 2825-2830.
33 (a) S. N. Magonov and D. H. Reneker, *Annu. Rev. Mater. Sci.*, 1997, **27**,175–222; (b) D. Z. Chen, R. M. Wang, I. Arachchige, G. Z. Mao and S. L. Brock, *J. Am. Chem. Soc.*, 2004, **126**, 16290-16291.
34 J. L. Serrano, Metallomesogens: Synthesis, Properties, and Application, Wiley-VCH, Weinheim, 1996.
35 (a) A. -M, Giroud-Godquin and P. M. Maitlis, *Angew. Chem. Int. Ed.*, 1991, **30**, 375-402; (b) S. A. Hudson and P. M. Maitlis, *Chem. Rev.*, 1993, **93**, 861-865.

Graphical Abstract for Table of Contents (TOC)

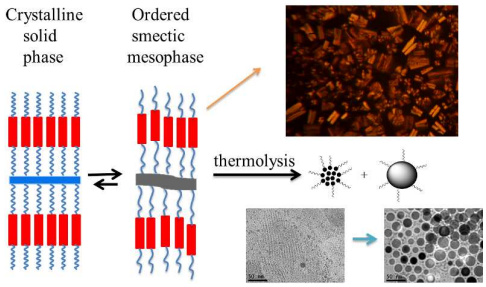

The mesogenic silver thiolate precursors provide an ideal two-dimensional confined platform for the fascinating controlled preparation of 2D shaped nanomaterials via the layered-precursor-to-lamellar-nanomaterial (LPLM) mechanism.